12th IFAC International Symposium on
Advanced Control of Chemical Processes
July 14-17, 2024. Toronto, Canada

Unstructured Dynamical Models for *S. cerevisiae* Cultures Fed With Glucose and Ammonium ⋆

Antoine Huet * **Mihaela Sbarciog** * **Philippe Bogaerts** *

* *3BIO-BioControl, Université Libre de Bruxelles, CP 165/61, 50, Av. F.-D. Roosevelt, B-1050 Brussels, Belgium (e-mail: antoine.huet@ulb.be; mihaela.iuliana.sbarciog@ulb.be; philippe.bogaerts@ulb.be).*

Abstract: This paper presents the development and the validation of two macroscopic growth models with coordinated uptake of glucose and ammonium for the yeast *Saccharomyces cerevisiae*. The two models differ in the structure chosen for the reaction kinetics: one employs generalized kinetic laws, the other employs extended Haldane laws. The predictions of both models are in agreement with experimental data, however, a slightly better accuracy can be noticed for the generalized kinetics formalism. This study emphasizes that an accurate, robust model captures the biological phenomena shown by the experimental data regardless of its structure and of the formalism used for its development.

Keywords: Saccharomyces cerevisiae, yeast growth, overflow metabolism, macroscopic dynamical model, kinetics, parameter identification

1. INTRODUCTION

Microorganisms have become real cell factories for the production of bio-based chemicals. Among these microorganisms, the yeast *Saccharomyces cerevisiae* is one of the workhorses of bioindustries (Henriques and Balsa-Canto, 2021), due to its common use especially in food, beverages and biofuel production. Additionally, there exists an extensive knowledge on *S. cerevisiae* physiology, molecular biology and genetics. However, in order to achieve favorable culture conditions and improved productivity, a macroscopic model is required, which relates the consumption of the most important nutrients to the yeast growth and metabolites production. While in the case of carbon-based nutrients, the model structure for the overflow metabolism proposed by Sonnleitner and Käppeli (1986) seems to be an accurate representation of the biological phenomena, less information is available on the influence of nitrogen-based nutrients.

Nitrogen, commonly supplied as ammonium to the culture, is an important nutrient for yeast growth. Several experimental studies emphasizing its importance are available (Larsson et al., 1993; Aon and Cortassa, 2001). Most of them establish that the carbon to nitrogen ratio in the constant feed supplied to a continuous culture is determinant for its steady state operation. However, high yeast concentrations are achieved in fed-batch operation, where the process does not reach a steady state but has a transient behavior. Hence, in a fed-batch yeast culture, unravelling the nitrogen influence on yeast growth and incorporating nitrogen dynamics in the yeast growth model is a must for an accurate prediction of the culture. However, most of the fed-batch models for yeast growth do not include nitrogen and assume that the yeast grows only utilizing a carbon source. To our knowledge, there are only a few modeling studies that consider the coordinated uptake of glucose and ammonium for yeast growth (Richelle et al., 2014; Robles-Rodríguez et al., 2018; Henriques and Balsa-Canto, 2021).

Robles-Rodríguez et al. (2018) developed two models for the oleaginous yeast *Yarrowia lipolytica* to predict the yeast growth and lipids accumulation. Both models include yeast overflow metabolism, but the first model relies only on extended Monod and Haldane kinetics while the second one employs also the Droop model to define the nitrogen uptake based on the internal nitrogen quota. Henriques and Balsa-Canto (2021) concluded that the Monod model is not sufficient to explain biomass formation in nitrogen-limited fermentations of *S. cerevisiae* during the winemaking process. They proposed two changes to the standard modeling approaches, where, on the one hand, the biomass growth accounts for protein and carbohydrates and, on the other hand, the fermentation rate is proportional to the total protein content.

For the use of *S. cerevisiae* in the food industry, Richelle et al. (2014) developed a growth model employing extended Monod kinetics, in which the uptake of nitrogen is modeled by a separate reaction mediated by the intracellular component alpha-ketoglutarate. Although the model predictions show good agreement with the experimental data, one may argue that this is not a macroscopic model in a strict sense as it involves an intracellular component which is not measured.

⋆ This research has been partially funded by the Wallonia Region (SPW Recherche) and supported by Wagralim, the agri-food innovation cluster in Wallonia Region, within the framework of the WA-SuNuP project.

The goal of this paper is to propose two macroscopic models with coordinated uptake of glucose and ammonium for the growth of *S. cerevisiae*. The two models differ in the structure chosen for the reaction kinetics: for the first model the kinetics are expressed as generalized kinetic laws, while for the second model the kinetics are expressed as extended Haldane laws. Both models are macroscopic models: the process dynamics depend only on extracellular components which are measured. The data sets used to identify the parameters of the models are the same as the ones used originally by Richelle et al. (2014). In a nutshell, the advantages of the new models compared to the model proposed by Richelle et al. (2014) may be summarized as: the new models have one reaction less, one state variable less, less stoichiometric and kinetic parameters while explaining the experimental data at least as accurately as the old model.

In an observability study (Sbarciog and Bogaerts, 2022) of the model proposed by Richelle et al. (2014), it was shown that the model is uniformly observable when two measurements are available only for the pairs i) glucose and ammonium and ii) glucose and ethanol. In an industrial setup and even at lab scale, on-line measurements of glucose and ammonium are not available (commonly glucose and ammonium are measured with enzymatic kits). On the contrary, the new models are globally uniformly observable when measurements of biomass and ethanol concentrations are available (developments not shown here due to space limitation). These measurements can be easily obtained by means of on-line probes. This is an important advantage provided by the structure of the new models, as the design and implementation of advanced optimization and control techniques require the availability of the full system state.

Last but not least, this study emphasizes that the obtained models are accurate and robust. The phenomena captured by the experimental data are dependent on the yeast metabolism triggered by the operational conditions but not on the chosen model structure.

The paper is organized as follows. Section 2 describes the biological background of the model and the chosen kinetic structures. Section 3 details the parameter identification and the results discussion and interpretation. Conclusions are drawn in Section 4.

2. MODEL DEVELOPMENT

2.1 Model structure

The well-known model proposed by Sonnleitner and Käppeli (1986) to describe the growth of *S. cerevisiae* relies on three reactions, of which two are purely oxidative and one purely reductive (Jouned et al., 2022):

Respiration on glucose

$$\mathrm{C_6H_{12}O_6} + \alpha_1\mathrm{O_2} + \alpha_2 n_\mathrm{N}[\mathrm{NH_3}] \rightarrow \alpha_2\mathrm{CH}_{n_\mathrm{H}}\mathrm{O}_{n_\mathrm{O}}\mathrm{N}_{n_\mathrm{N}} + \alpha_3\mathrm{CO_2} + \alpha_4\mathrm{H_2O} \quad (1)$$

Fermentation

$$\mathrm{C_6H_{12}O_6} + \alpha_5 n_\mathrm{N}[\mathrm{NH_3}] \rightarrow \alpha_5\mathrm{CH}_{n_\mathrm{H}}\mathrm{O}_{n_\mathrm{O}}\mathrm{N}_{n_\mathrm{N}} + \alpha_6\mathrm{CO_2} + \alpha_7\mathrm{H_2O} + \alpha_8\mathrm{C_2H_6O} \quad (2)$$

Respiration on ethanol

$$\mathrm{C_2H_6O} + \alpha_9\mathrm{O_2} + \alpha_{10} n_\mathrm{N}[\mathrm{NH_3}] \rightarrow \alpha_{10}\mathrm{CH}_{n_\mathrm{H}}\mathrm{O}_{n_\mathrm{O}}\mathrm{N}_{n_\mathrm{N}} + \alpha_{11}\mathrm{CO_2} + \alpha_{12}\mathrm{H_2O} \quad (3)$$

In the reactions (1)-(3), $\mathrm{CH}_{n_\mathrm{H}}\mathrm{O}_{n_\mathrm{O}}\mathrm{N}_{n_\mathrm{N}}$ denotes the biomass, whose molecular composition (n_H,n_O,n_N) is determined from an elemental analysis of the dried biomass, while α_i, $i = 1 \dots 12$, are stoichiometric parameters.

A simplified reaction network, derived from (1)-(3), is employed for the models development:

$$G + k_5 N \xrightarrow{r_1} k_1 X \quad (4)$$

$$G + k_6 N \xrightarrow{r_2} k_2 X + k_4 E \quad (5)$$

$$E + k_7 N \xrightarrow{r_3} k_3 X \quad (6)$$

X, G, N and E are respectively biomass, glucose, ammonium and ethanol; k_i, $i = 1 \dots 7$, are pseudo-stoichiometric coefficients; r_j, $j = 1 \dots 3$ are respectively the reaction rates of glucose oxidation, fermentation and ethanol oxidation. Further on, it is assumed that oxygen is supplied in excess and does not limit the growth.

The mass balance equations, which describe the time evolution of component concentrations in a fed-batch operated bioreactor, read as follows:

$$\frac{dX}{dt} = k_1 r_1 X + k_2 r_2 X + k_3 r_3 X - \frac{F}{V} X \quad (7)$$

$$\frac{dG}{dt} = -r_1 X - r_2 X + \frac{F}{V}(G_{in} - G) \quad (8)$$

$$\frac{dN}{dt} = -k_5 r_1 X - k_6 r_2 X - k_7 r_3 X + \frac{F}{V}(N_{in} - N) \quad (9)$$

$$\frac{dE}{dt} = k_4 r_2 X - r_3 X - \frac{F}{V} E \quad (10)$$

$$\frac{dV}{dt} = F \quad (11)$$

where X, G, N, E stand for the concentrations of the above mentioned components; r_1, r_2 and r_3 respectively represent the reaction rates of respiration, fermentation and ethanol oxidation; V is the reactor volume; F denotes the feedflow rate, which contains both glucose and ammonium, with concentrations G_{in} and N_{in}.

The reaction rates describing the overflow metabolism have the same structure as defined in the seminal work of Sonnleitner and Käppeli (1986)

$$r_1 = \min(r_G, r_O) \quad (12)$$

$$r_2 = \max(0, r_G - r_O) \quad (13)$$

$$r_3 = \max(0, (r_O - r_G)\, E/(E + K_E)) \quad (14)$$

where r_O denotes the maximum respiration rate and r_G denotes the glucose uptake rate. r_O is implicitly rescaled in the same units as r_G (gG/gX/h). Note that the factor $E/(E + K_E)$ is included in the ethanol oxidation rate (14) as a physical constraint: consumption of ethanol cannot occur when ethanol is depleted. Hence, the parameter K_E will not be identified from data but fixed to an arbitrary low value ($K_E = 0.1$ gE/L). Finally, the scaling factor that should be considered in (14) to pass from units in gG/gX/h to units in gE/gX/h is set to 1 gE/gG, as proposed in Richelle et al. (2014).

2.2 Reaction rates

Commonly, the reaction kinetics of bioprocesses are chosen as extended Monod or Haldane laws, which are given as a product of factors expressing the limiting and the inhibiting features of the components involved in a particular reaction. While in the case of extended Monod laws the limiting effect of a component is modeled with a classical

Monod factor and the inhibiting effect with a separate hyperbolic factor, in the case of Haldane laws these effects are combined in only one factor.

Although less employed, generalized kinetic laws are a useful tool for modeling the reaction kinetics of bioprocesses. They express the impact of a component on the reaction kinetics in terms of activation and deactivation and they are particularly appealing as this formalism avoids the local identifiability problems of extended Monod laws (Mairet and Bernard, 2019) and can even be rigorously linearized with respect to the parameters when the reaction rate values can be estimated (Bogaerts et al., 1999; Richelle and Bogaerts, 2015).

Recall that one of the goals of this study is to reveal the influence of ammonium on the respiration and glucose uptake rates. To this end, our investigation starts with general structures detailed in the next subsections and model reduction is performed based on the parameter identification results.

Generalized kinetic laws The initial rates in the generalized kinetic laws formalism are chosen as follows:

$$\begin{aligned} r_{O,gen} &= \alpha_O \cdot N^{\alpha_{NO}} exp(-\beta_{NO} \cdot N) \\ r_{G,gen} &= \alpha_G \cdot G^{\alpha_{GG}} exp(-\beta_{GG} \cdot G) N^{\alpha_{NG}} exp(-\beta_{NG} \cdot N) \end{aligned} \tag{15}$$

where α_O, α_{NO}, β_{NO}, α_G, α_{GG}, β_{GG}, α_{NG} and β_{NG} are parameters that will be estimated from the experimental data.

The rates (15) express that ammonium concentration N has an activation and deactivation influence on the maximum respiration capacity r_O, while both nutrients, glucose and ammonium, activate and deactivate the glucose uptake rate r_G. It is assumed that the glucose concentration does not influence the maximum respiration capacity, which is in agreement with modeling yeast growth studies published so far.

Generalized Haldane laws Considering similar effects of glucose and ammonium on the respiration and glucose uptake rates, these can be rewritten in the extended Haldane formalism as:

$$\begin{aligned} r_{O,Hal} &= \mu_O \frac{N}{K_{NO} + N + K_{iNO} N^2} \\ r_{G,Hal} &= \mu_G \frac{G}{K_{GG} + G + K_{iGG} G^2} \frac{N}{K_{NG} + N + K_{iNG} N^2} \end{aligned} \tag{16}$$

where μ_O, K_{NO}, K_{iNO}, μ_G, K_{GG}, K_{iGG}, K_{NG} and K_{iNG} are parameters that will be estimated from experimental data.

3. PARAMETER ESTIMATION AND MODEL REDUCTION

All model parameters, comprising the stoichiometric and the kinetic parameters, are estimated based on experimental data. The experimental data sets are the same as described by Richelle et al. (2014). This experimental database consists of four *S. cerevisiae* fed-batch culture experiments, which were performed to emphasize the influence of different ammonium concentration levels in the culture medium. Therefore, they mostly differ by the ammonium and glucose concentration in the feeding.

All experiments last for 21 hours and measurements for each state variable (X, G, N and E) were made at 15 or 16 time instants per experiment. The identification of model parameters is performed by using the trust-region-reflective optimization algorithm (function `lsqnonlin` in MATLAB) in order to minimize a least-squares criterion. The criterion is built as the sum of squared differences between the result of the model simulation and the experimental values. The squared difference is weighted by the inverse of the variance of the measurement error for each experimental measurement. The standard deviation for each measurement was either set to the one proposed by the protocol, or computed at a higher value by Richelle et al. (2014). The standard deviations associated with the biomass, glucose, ammonium and ethanol measurement protocols are, respectively, 0.5 g/L, 0.2 g/L, 0.45 g/L and 0.1 g/L. The resulting criterion is expressed as follows

$$\text{SSE}(\theta) = \Sigma_{j=1}^{n} \Sigma_{i=1}^{N_j} \left(\hat{y}_{ij}(\theta) - y_{ij}\right)^T Q_{ij}^{-1} \left(\hat{y}_{ij}(\theta) - y_{ij}\right) \tag{17}$$

where θ is the parameters vector with $dim(\theta) = 15$, which, depending on the kinetic structure employed, assumes one of the forms

$$\theta_{gen}^T = [\, k_1 \;\; k_2 \;\; k_3 \;\; k_4 \;\; k_5 \;\; k_6 \;\; k_7 \;\; \alpha_O \;\; \alpha_{NO} \;\; \beta_{NO} \;\; \alpha_G \;\; \alpha_{GG} \;\; \beta_{GG} \;\; \alpha_{NG} \;\; \beta_{NG} \,] \tag{18}$$

$$\theta_{Hal}^T = [\, k_1 \;\; k_2 \;\; k_3 \;\; k_4 \;\; k_5 \;\; k_6 \;\; k_7 \;\; \mu_O \;\; K_{NO} \;\; K_{iNO} \;\; \mu_G \;\; K_{GG} \;\; K_{iGG} \;\; K_{NG} \;\; K_{iNG} \,] \tag{19}$$

$\hat{y}_{ij}(\theta) = \left[\, \hat{X}_{ij} \;\; \hat{G}_{ij} \;\; \hat{N}_{ij} \;\; \hat{E}_{ij} \,\right]^T$ is the vector of predicted state variables at the ith time instant of the jth experiment, while $y_{ij} = [\, X_{ij} \;\; G_{ij} \;\; N_{ij} \;\; E_{ij} \,]^T$ is the vector of the corresponding experimental measurements. Q_{ij} is a positive definite symmetric weighting matrix, defined as

$$Q_{ij} = \text{diag}\left(\sigma^2(X_{ij}), \sigma^2(G_{ij}), \sigma^2(N_{ij}), \sigma^2(E_{ij})\right)$$

where σ^2 represents the variance of the associated measurement errors.

The optimization of the cost index (17) is usually cumbersome due to the existence of several local minima. To circumvent this issue, a multistart approach is employed, in which parameters are initialized at 15 different values in a properly chosen parameter range. The chosen range for each parameter is given in Table 1 for the generalized kinetics and in Table 2 for the extended Haldane formalism.

In a first step, the parameter sets θ_{gen} and θ_{Hal} as defined in (18) and (19) are identified using all four available data sets. A first set of observations, common to both generalized kinetics and extended Haldane formalisms, is made on the pseudo-stoichiometric coefficients k_6 and k_7. First looking at k_6, which is linked to ammonium consumption in the fermentation reaction (5), the identified value is 0.0005 with a variation coefficient of 285.17% in the generalized kinetic formalism, and 8.12E-06 with a variation coefficient of 6917% in the extended Haldane formalism. In the case of k_7, which is linked to ammonium consumption in the ethanol respiration reaction (6), the identified value is 0.0002 with a variation coefficient of 95.38% in the generalized kinetic formalism, and 0.0061 with a variation coefficient of 7.74% in the extended Haldane formalism. While the values are different, they are not significant compared to the magnitude of the other stoichiometric coefficients. Based on these observations, a first model reduction is performed, which consists in

Table 1. Estimated parameters for the generalized kinetic formalism

Parameter	Range of initialization	Set 1 Experiments 1-2-3-4	Set 2 Experiments 1-2-3	Set 3 Experiments 1-2-4	Set 4 Experiments 1-3-4	Set 5 Experiments 2-3-4	Variation coefficients*
k_1	0.1-1	0.6237	0.6237	0.5575	0.6237	0.5717	17.72
k_2	0.1-1	0.1987	0.1987	0.1959	0.1987	0.1990	5.30
k_3	0.1-1	4.9609	4.9609	5.3309	4.9609	4.9394	16.18
k_4	0.1-1	0.1905	0.1905	0.1740	0.1905	0.2050	3.04
k_5	0.1-1	0.6071	0.6071	0.5939	0.6071	0.5852	7.77
α_O	0.01-0.1	0.1468	0.1468	0.1460	0.1468	0.1425	17.02
α_{NO}	0.1-1	1.1988	1.1988	1.1992	1.1988	1.1346	3.06
β_{NO}	0.1-1	0.4957	0.4957	0.4779	0.4957	0.4395	14.42
α_G	1-10	2.8719	2.8719	2.8773	2.8719	2.8283	3.22
α_{NG}	0.1-1	0.4076	0.4076	0.4235	0.4076	0.3212	10.08
α_{GG}	0.1-1	0.8798	0.8798	0.9233	0.8798	0.7575	0.0005
β_{GG}	0.1-1	0.2171	0.2171	0.2221	0.2171	0.2296	0.0014
SSE*	/	2029.1	2029.1	2137.6	2028.9	2526.1	/

* calculated for Set 1

Table 2. Estimated parameters for the extended Haldane formalism

Parameter	Range of initialization	Set 1 Experiments 1-2-3-4	Set 2 Experiments 1-2-3	Set 3 Experiments 1-2-4	Set 4 Experiments 1-3-4	Set 5 Experiments 2-3-4	Variation coefficients*
k_1	0.1-1	0.5625	0.6491	0.6211	0.4896	0.4088	22.59
k_2	0.1-1	0.2007	0.2042	0.2074	0.2097	0.2066	5.61
k_3	0.1-1	5.9651	6.8832	6.4176	6.8881	5.9399	11.61
k_4	0.1-1	0.1901	0.1881	0.1722	0.1895	0.2219	3.86
k_5	0.1-1	0.5229	0.5325	0.5192	0.4846	0.3893	15.78
μ_O	1-10	1.7668	1.8346	1.5616	1.5055	1.6988	22.85
K_{NO}	1-10	19.5118	21.7647	19.3322	15.9762	14.6827	17.13
μ_G	10-20	103.9667	95.3629	116.7020	108.9475	110.6228	10.76
K_{GG}	1-10	49.9465	40.6227	52.2778	53.9093	50.4307	9.41
K_{iGG}	0.1-1	0.8480	0.1014	0.3388	0.1118	0.1642	21.93
K_{NG}	0.1-1	0.1705	0.3752	0.3595	0.3012	0.2038	24.47
SSE*	/	2486.9	2347.6	2581.2	2346.2	3260.2	/

* calculated for Set 1

removing the ammonium consumption terms in both the fermentation reaction (5) and in the ethanol respiration reaction (6). This does not mean that biologically there is no coordinated consumption of ammonium when the yeast ferments or when it respires ethanol. However, in our data sets, the ammonium consumption during the fermentation is negligible. The ammonium consumption during ethanol respiration is also negligible, and this small amount is accounted for in the glucose respiration, which occurs simultaneously with ethanol respiration (pure respiration regime).

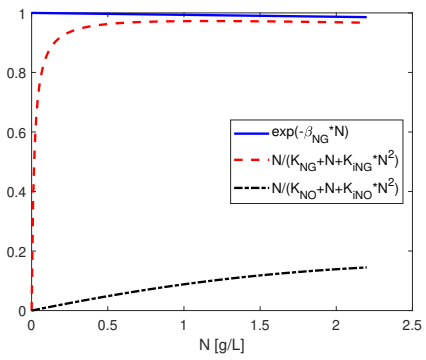

Fig. 1. Evolution of the factors considered for model reduction as function of ammonium concentration

Other parameters in θ_{gen} and θ_{Hal} that are considered for model reduction are β_{NG} in the generalized kinetics formalism and K_{iNG} and K_{iNO} in the extended Haldane formalism. The estimated values are 0.0065 for β_{NG}, 0.0121 for K_{iNG} and 0.6890 for K_{iNO}. Since a parameter cannot be removed from a model without checking its contribution to the kinetic rate, we evaluated the factors $exp(-\beta_{NG} \cdot N)$, $\frac{N}{K_{NG}+N+K_{iNG}N^2}$ and $\frac{N}{K_{NO}+N+K_{iNO}N^2}$ for the ammonium concentration range [0, 2.2] g/L, which is the range of ammonium variation in the experimental data. As Figure 1 shows, the exponential factor involving β_{NG} is practically equal to one for the whole range of ammonium, while no ammonium inhibition effect for any of the Haldane factors is visible, which implies that these factors can be replaced with Monod factors. Subsequently, the expression of the kinetic rates for each formalism and the associated parameter vectors become:

$$
\begin{aligned}
r_{O,gen} &= \alpha_O \cdot N^{\alpha_{NO}} exp(-\beta_{NO} \cdot N) \\
r_{G,gen} &= \alpha_G \cdot G^{\alpha_{GG}} exp(-\beta_{GG} \cdot G) N^{\alpha_{NG}} \\
r_{O,Hal} &= \mu_O \frac{N}{K_{NO}+N} \\
r_{G,Hal} &= \mu_G \frac{G}{K_{GG}+G+K_{iGG}G^2} \frac{N}{K_{NG}+N} \\
\theta_{gen}^T &= [\, k_1 \;\; k_2 \;\; k_3 \;\; k_4 \;\; k_5 \;\; \alpha_O \;\; \alpha_{NO} \;\; \beta_{NO} \;\; \alpha_G \;\; \alpha_{GG} \;\; \beta_{GG} \;\; \alpha_{NG} \,] \\
\theta_{Hal}^T &= [\, k_1 \;\; k_2 \;\; k_3 \;\; k_4 \;\; k_5 \;\; \mu_O \;\; K_{NO} \;\; \mu_G \;\; K_{GG} \;\; K_{iGG} \;\; K_{NG} \,]
\end{aligned}
\tag{20}
$$

Next, the parameters of the reduced models are identified using all four experiments (data Set 1) or combination of three experiments (data Set 2, Set 3, Set 4 and Set 5). The estimated values and variation coefficients are presented in Table 1 for the generalized kinetic laws and in Table 2 for

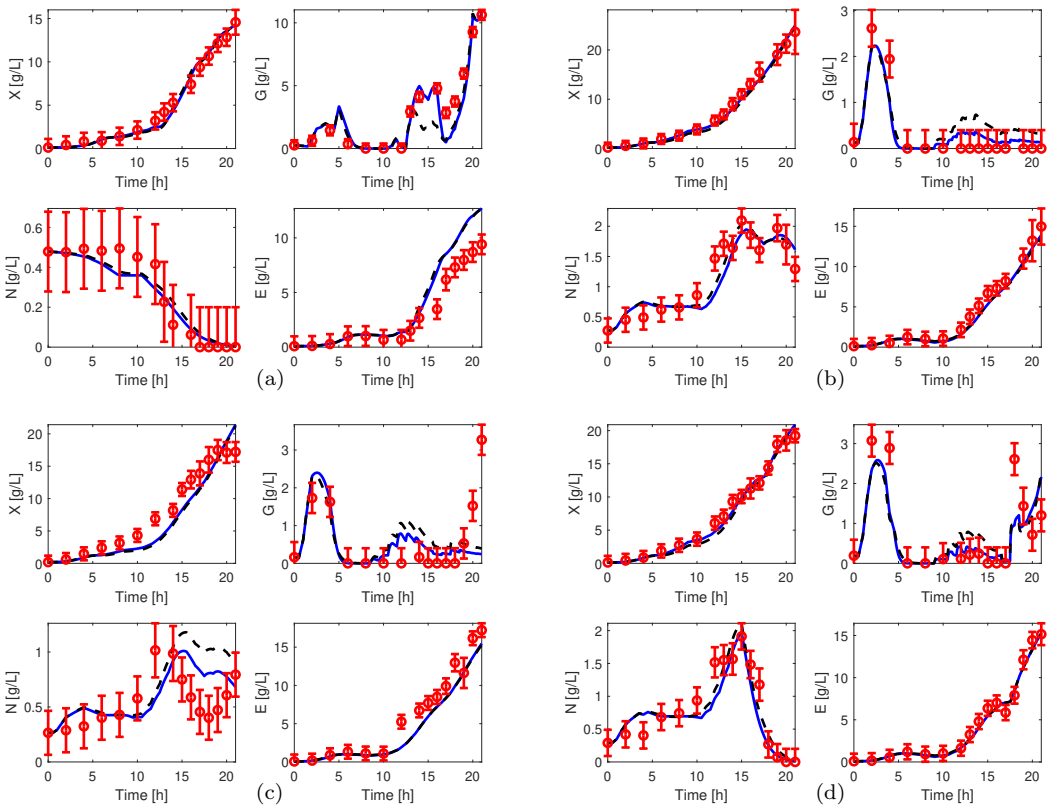

Fig. 2. Direct validation: red dots - experimental data, continuous blue line - model predictions (generalized kinetic formalism), dashed black line - model predictions (extended Haldane formalism). (a) - Experiment 1, (b) - Experiment 2, (c) - Experiment 3, (d) - Experiment 4

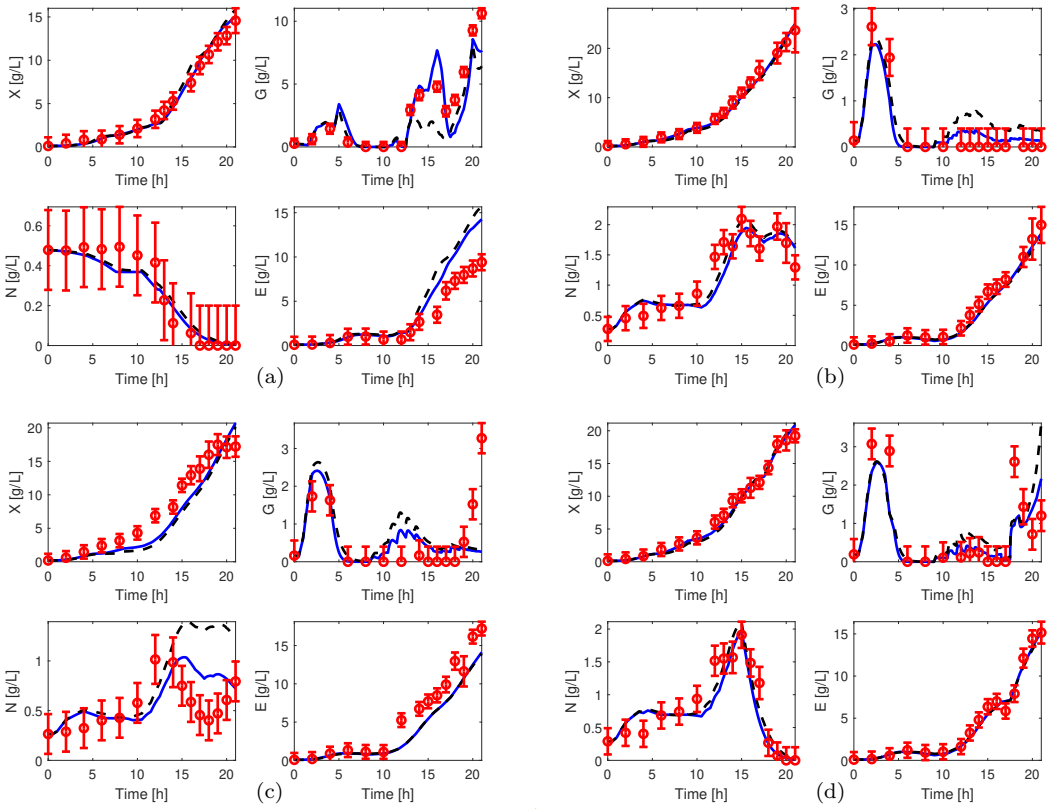

Fig. 3. Leave-one-out cross validation: red dots - experimental data, continuous blue line - model predictions (generalized kinetic formalism), dashed black line - model predictions (extended Haldane formalism). (a) - Experiment 1 (Set 2), (b) - Experiment 2 (Set 3), (c) - Experiment 3 (Set 4), (d) - Experiment 4 (Set 5)

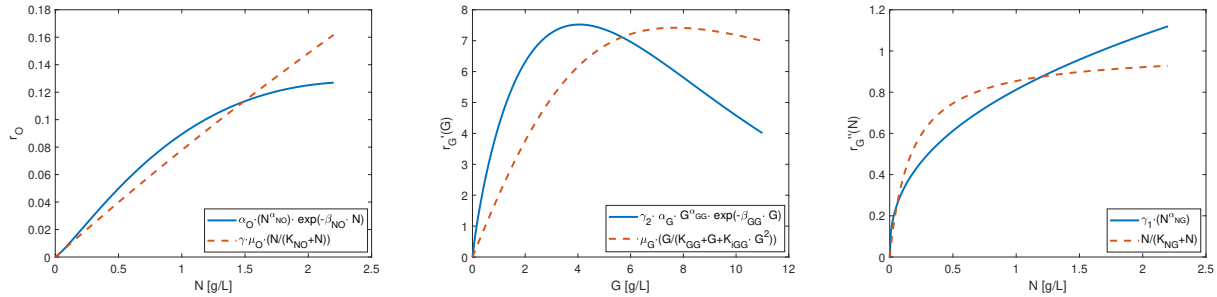

Fig. 4. Qualitative comparison of the effects of N on r_O (left), G on r_G (center) and N on r_G (right) with both kinetic formalisms. In each case, the two curves are rescaled such that they have the same average value.

the extended Haldane laws. Further on, Figure 2 presents the direct validation of the two models with the parameter values identified using data Set 1, while Figure 3 shows the cross validation for the leave-one-out approach, where the model is validated with the experimental data set which was not used for identification.

Although the kinetic structures are different, the predictions of both models using the parameters estimated with data Set 1 are close. However, the generalized kinetic model provides a more accurate prediction of all state variables compared to the extended Haldane model. This is particularly obvious in the simulation of the glucose concentration in Experiment 1 between 12 and 17h, where the extended Haldane model, although having an accurate trend, does not manage to predict sufficiently the intermediate glucose accumulation. A second significant difference between the two models is seen in the simulation of ammonium in Experiment 3, between 12 and 21h. Here, the extended Haldane model shows exactly the same trend as the generalized kinetic model, but it is not able to express well the ammonium consumption. It should be noted that in both cases, this particular dynamic is not well captured. Both models also fail to predict the final glucose accumulation from Experiment 3 (18 to 21h). However, the other signals present trends that match most of the time the experimental measurements.

The observations made for direct validation also hold for cross validation (Figure 3). Although the predictions are not as good as in direct validation, both models provide a reasonable approximation of the experimental data set that was not used for identification. However, larger confidence intervals on the parameters of the extended Haldane model are obtained.

To investigate to which extent the kinetic rates of the two models capture the same phenomena, their respective variation in function of each substrate are displayed in Figure 4. A visual comparison of these curves shows that ammonium has a limiting effect on the maximum respiration rate and on the glucose uptake rate, while glucose has both limiting and inhibiting effects on the glucose uptake rate. These effects are clearly expressed by each of the two kinetic models, leading to the conclusion that the same biological evidence shown by the experimental data is captured by both kinetic structures.

4. CONCLUSIONS

In this paper two macroscopic models with coordinated uptake of glucose and ammonium that characterize the growth of *Saccharomyces cerevisiae* were developed. The emphasis was on unravelling the influence of ammonium on the kinetic rates. The results show that ammonium has a limiting effect on both maximum respiration rate and glucose uptake rate. Although using different formalisms to model the kinetic rates, both models predict well the biological phenomena shown by the experimental data.

REFERENCES

Aon, J. and Cortassa, S. (2001). Involvement of nitrogen metabolism in the triggering of ethanol fermentation in aerobic chemostat cultures of *Saccharomyces cerevisiae*. *Metab. Eng.*, 3, 250–264.

Bogaerts, Ph., Castillo, J., and Hanus, R. (1999). A general mathematical modelling technique for bioprocesses in engineering applications. *System Analysis Modeling Simulation*, 35, 87–113.

Henriques, D. and Balsa-Canto, E. (2021). The Monod model is insufficient to explain biomass growth in nitrogen-limited yeast fermentation. *Appl. Environ. Microbiol.*, 87, e01084–21.

Jouned, M., Kager, J., Herwig, C., and Barz, T. (2022). Event driven modeling for the accurate identification of metabolic switches in fed-batch culture of *S. cerevisiae*. *Biochem. Eng. J.*, 180, 108345.

Larsson, C., von Stockar, U., Marison, I., and Gustafsson, L. (1993). Growth and metabolism of *Saccharomyces cerevisiae* in chemostat cultures under carbon-, nitrogen-, or carbon- and nitrogen-limiting conditions. *J. Bacteriol.*, 175, 4809–4816.

Mairet, F. and Bernard, O. (2019). Twelve quick tips for designing sound dynamical models for bioprocesses. *PLoS Comput Biol*, 15(8), e1007222.

Richelle, A. and Bogaerts, Ph. (2015). Systematic methodology for bioprocess model identification based on generalized kinetic functions. *Biochem. Eng. J.*, 100, 41–49.

Richelle, A., Fickers, P., and Bogaerts, Ph. (2014). Macroscopic modelling of baker's yeast production in fed-batch cultures and its link with trehalose production. *Comput. Chem. Eng.*, 61, 220–233.

Robles-Rodríguez, C., Munoz-Tamayo, R., Bideaux, C., Gorret, N., Guillouet, S., Molina-Jouve, C., Roux, G., and Aceves-Lara, C. (2018). Modeling and optimization of lipid accumulation by *Yarrowia lipolytica* from glucose under nitrogen depletion conditions. *Biotechnol. Bioeng.*, 115, 1137–1151.

Sbarciog, M. and Bogaerts, Ph. (2022). Observability and observers for baker's yeast growth with coordinated uptake of glucose and ammonium. In *ICSTCC - Proceedings 2022*, 86–91. IEEE, Sinaia, Romania.

Sonnleitner, B. and Käppeli, O. (1986). Growth of *Saccharomyces cerevisiae* is controlled by its limited capacity: formulation and verification of a hypothesis. *Biotechnol. Bioeng.*, 28, 927–937.